JOURNAL OF THERMOPHYSICS AND HEAT TRANSFER
Vol. 21, No. 2, April–June 2007

Heat Transfer Model for Blade Twist Actuator System

Nicholas Caldwell* and Ephraim Gutmark†
University of Cincinnati, Cincinnati, Ohio 45221
and
Robert Ruggeri‡
Boeing Phantom Works, Kent, Washington 98032

DOI: 10.2514/1.23120

A lumped mass heat transfer model is developed for a blade twist actuator system that uses thermally activated shape memory alloys to alter the shape of a wing. These alloys are coupled with thermoelectric modules that supply the heat necessary to activate the shape alteration characteristics of the material. The model predicts the unsteady temperatures in different portions of the actuator system, and comparisons between experimental data and the heat transfer model are made. Furthermore, parametric studies are made of system variables to optimize the numerical model, and the effect of each variable on the comparison is examined. Differences between the numerical and experimental models are discussed, and efforts are made to minimize this difference through variations in the numerical variables. The potential for using this technology to increase range and payload of aircraft is discussed.

Nomenclature

c_p	=	specific heat, J/kg · K
h	=	convective heat transfer coefficient, W/K
I	=	electrical current, A
N	=	number of thermoelectric modules in row
n	=	number of time steps
q	=	heat flow, W
R	=	electrical resistance, Ω
T	=	temperature of thermal zone or atmosphere, °C
t	=	time, s
α	=	Peltier coefficient, V/K
Δt	=	time step, s
κ	=	thermal conductivity, W/K

I. Introduction

THE shape of an aircraft component is typically designed for optimum performance at only one specific flight condition, and its shape is unchangeable. This results in aerodynamic losses at flight conditions other than the design point. By optimizing aerodynamic surfaces at other flight conditions, aircraft range and payload capabilities can be improved significantly. Shape optimization of turbomachinery and inlets could also improve engine performance characteristics.

One manner in which aerodynamic surfaces can be reshaped is with shape memory alloys (SMAs). The shape of SMAs responds to changes in temperature. For example, shape memory alloys can be trained to twist as their temperature changes. The SMA has a large specific work output, and lightweight composite structures can be made using this material. By properly designing a composite structure, its shape can be changed as desired to optimize for different flight conditions. In this manner an engine inlet can be designed to be efficient at both takeoff and cruise conditions, or a wing could be twisted to fly at different altitudes without a major performance loss. This study examines a system that can twist a wing by means of a NiTinol shape memory alloy that is thermally activated when current is applied to thermoelectric modules (TEMs). A mathematical model for the heat transfer occurring within the system is developed, and simulation results show how the temperature of the NiTinol changes with time when the TEMs are subjected to a specified current profile.

Thermoelectric modules have frequently been used in the past to perform a number of functions associated with the control of sensor temperatures, cold probes, freezers, sensor calibrators, and constant-temperature chambers [1]. The key characteristics of TEMs that make them particularly useful are their ability to cool below the temperature of the thermal ground and their ease of temperature control. Applying TEMs to thermally actuate shape memory alloy takes advantage of these primary characteristics, but applies them in an unconventional way.

This concept uses TEMs to control the temperature of two SMA tubes by heating one while maintaining the other tube at a temperature below its shape memory transition temperature. The direction of actuator rotation is reversed by reversing the direction of current flow, thereby heating the cold NiTinol tube and cooling the warm one.

TEMs are essentially a pair of PN junctions (a PN junction is a combination of a P-type semiconductor with an N-type semiconductor in close contact) that exhibit characteristics similar to a pair of thermocouple junctions. However, instead of relying on a temperature difference to generate a voltage (the Seebeck effect), the Peltier effect is employed in which power (current) is applied across a pair of junctions, and heat flows from one junction (the cooling body) to the other (the warming body). It is this ability of TEMs to easily reverse the direction of heat flow that makes them highly effective as a method of alternately heating and cooling the NiTinol tubes.

Systems have been investigated that used only resistance heaters and passive cooling instead of TEMs to control the temperature of the NiTinol tubes [2]. The current application requires rapid cooling, implying low thermal resistance, high heat loss, and low thermal efficiency when resistance heaters are used. The use of TEMs to heat and cool the actuator increases thermal efficiency and reduces the total quantity of waste heat produced. This is the most significant advantage of TEMs in our application. Six to eight times more power is required for a passively cooled actuator than for one using TEMs in a full-scale actuator application. The increased power requires a larger area for heat dissipation, and it adds significant mass to the system. For these reasons TEMs have been used as the primary means of heating as well as cooling this actuator. The alternate heating and cooling of a pair of objects is an ideal use of TEMs. It

Presented as Paper 0982 at the 44th AIAA Aerospace Sciences Meeting and Exhibit, Reno, Nevada, 9–12 January 2006; received 24 February 2006; accepted for publication 2 September 2006.

*Graduate Research Assistant, Department of Aerospace Engineering, ML0070. Student Member AIAA.
†Professor and Ohio Eminent Scholar, Department of Aerospace Engineering, ML0070. Associate Fellow AIAA.
‡Technical Fellow, MS 4A-51, Seattle, WA 98124. Member AIAA.

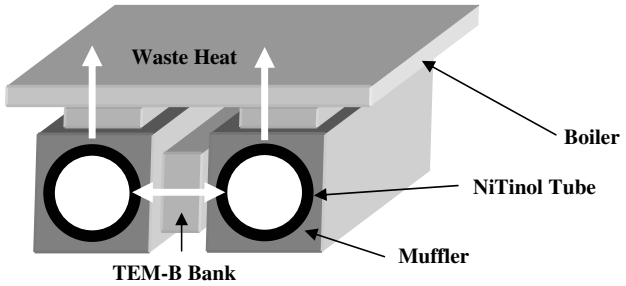

Fig. 1 Simplified system model.

takes advantage of their strengths and results in an extremely lightweight, rugged, solid-state actuator. Figure 1 illustrates the simplified model of the system.

II. Experimental Setup

The experimental setup is a quarter-scale model of a system that could be implemented on an aircraft. Hollow tubes composed of NiTinol shape memory alloy approximately 5 in. long are inserted into aluminum housings separated by a bank of TEMs. The thermoelectric modules employed in this study are manufactured by T. E. Technologies in Traverse City, Michigan, Model no. TM-2829, with physical dimensions 7.5 mm × 22 mm. A pair of tubes each inside a housing (thermal muffler) comprises the actuator as shown in Fig. 2. A carbon velvet interface conducts heat from the muffler to the NiTinol tube inside. The TEMs pump heat between adjacent mufflers (NiTinol tubes) instead of heating and cooling each one independently. This approach conserves the thermal energy in the NiTinol tubes.

Three banks of TEMs are used in the actuator, as illustrated in Fig. 2. The interior bank transfers heat between the two mufflers and are referred to as the shuttle bank of TEMs. The two additional TEM banks, hereafter referred to as guards, control heat flow between each muffler and the boiler (thermal ground). They are used to manage the average temperature of the system and dissipate waste heat to air through the boiler. Input current through the guard banks of TEMs is limited to ±2.5 A at an actuation voltage of 7 V, while the shuttle bank can maintain ±3.0 A at 10 V. The TEMs and aluminum mufflers are shown in Fig. 2, but the NiTinol tubes cannot be seen. The boiler is clearly visible in the photograph in Fig. 2. It is a metal structure that supports a pair of finned heat sinks and cooling fans (not shown) that circulate ambient air to cool the system.

The data reported in this paper have been obtained from a 1/4-scale actuator assembled in a benchtop test configuration. In an aircraft, the actuator would be completely surrounded by thermal insulation and heat dissipation would be through a cooling system. A benchtop cooling system has been set up that simulates the on-aircraft conditions. The overall heat transfer coefficient of the test apparatus is estimated to be approximately that required on the aircraft. The outside of the actuator was exposed to air during these tests and was not thermally insulated. Subsequent testing and analysis will be performed to estimate the significance of thermal losses to the air during these tests.

The three banks of TEMs are powered by direct current, with each bank supplied by an independent power supply. The power supplies

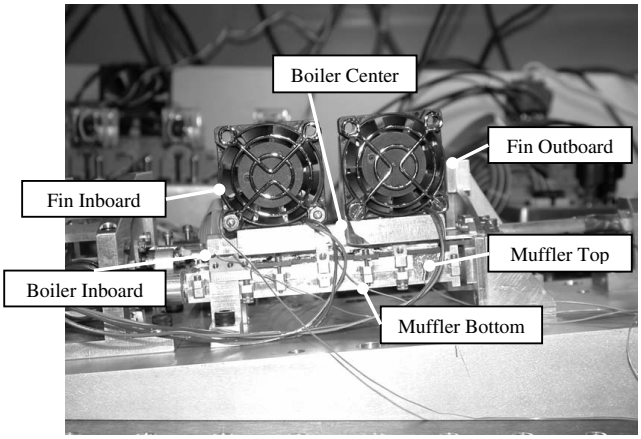

Fig. 3 Thermocouple locations on quarter-scale actuator.

act as the current controller, and a computer provides set-point instructions regulating the current level. Temperatures are determined by scanning several type-K thermocouples at regular intervals. In this test the scan interval is approximately 5 s, with thermocouple locations shown in Fig. 3. Measurements relevant to the numerical comparisons are taken at multiple muffler locations and at two points on the boiler. Each thermocouple measurement has an uncertainty of ±0.3°C. Temperature measurements of the NiTinol material itself have a larger margin of error, averaging approximately ±5°C. This is due to the fact that thermocouples cannot be securely fastened to the NiTinol material which is undergoing mechanical action. However, numerical comparisons made in this paper do not reflect comparisons with NiTinol tube temperature, but with muffler and boiler temperatures. Estimates of NiTinol tube temperature may be made knowing the conduction coefficient between the aluminum mufflers and the NiTinol material.

The cooling system consists of cooling fins and a pair of cooling fans that circulate ambient laboratory air.

III. Experimental Results

Four cases of experimental results are presented in this section. The first three are simplified cases in which only one bank of TEMs is powered. The fourth case is a complex power profile that consecutively forces the left and right SMA tubes above the austenitic temperature, showing that the actuator can be cycled between two shapes within the required time. For the actuation currents reported in this paper, the NiTinol tubes deflect approximately ±40°, though much higher angular deflections have been achieved.

A. Case 1—Left Guard TEM Bank Actuated

This case involves the left bank of guard TEMs undergoing a simple current profile, shown in Fig. 4. The TEMs receive a current of +1 A for a period of 560 s after which the current is removed. After a quiescent period during which the system cools, an opposite current of −1 A is applied to the same TEM bank. All other TEM rows remain idle during the entire test, as shown in Fig. 4. Thermocouples placed on the two aluminum mufflers show how the

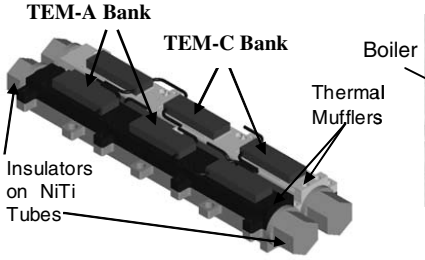

Drawing of TEM's and Actuator Mufflers

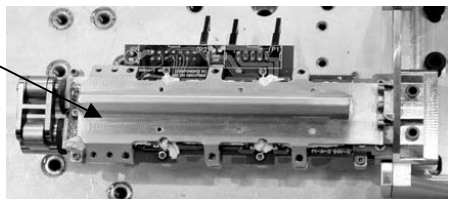

Assembled Actuator & Boiler without Fans

Fig. 2 Solid model and photograph of actuator system.

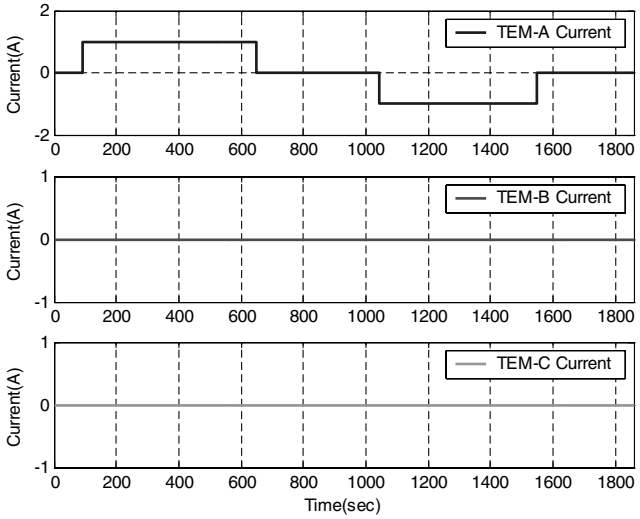

Fig. 4 Input current profile for case 1.

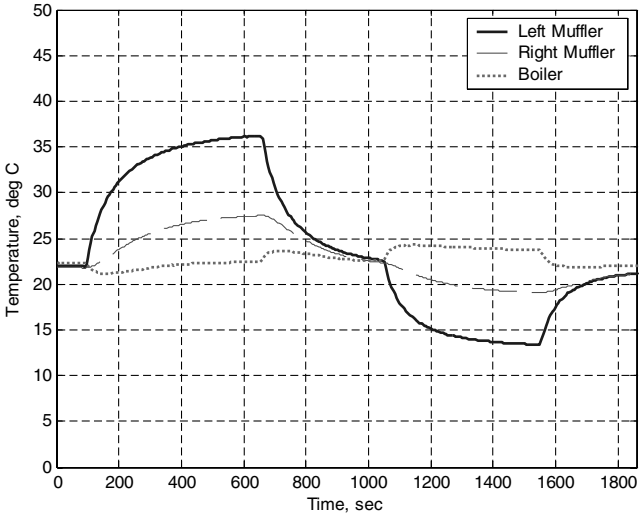

Fig. 5 Temperature response resulting from case 1 input current profile.

temperatures are affected by the current profiles. Because of the initially positive current profile on the left guard TEM bank, heat is transferred from the left side of the boiler to the left muffler. Shown in Fig. 5, this results in a temperature increase of the left muffler and a temperature decrease of the boiler. Through conduction alone, a slight temperature rise is also experienced by the right muffler. Heat is transferred from the mufflers to the NiTinol tubes by conduction. Therefore, the temperature increase of a muffler heats the appropriate NiTinol tube, which twists as a result of its temperature change.

B. Case 2—Right Guard TEM Bank Actuated

The second case under investigation looks at the effect on the system of activating only the right guard bank of TEMs. The input current profile is similar to that shown in Fig. 4 except that the right guard bank is actuated. The magnitude is the same as that in case 1, but the initial current is negative instead of positive. The temperature response shown in Fig. 6 is similar to that in Fig. 4. Because the initial current applied to the right guard bank of TEMs is negative, heat is being transferred from the right muffler to the right side of the boiler. Hence the boiler temperature experiences a slight temperature rise which depends upon its thermal capacity, and at the same time the temperature of the right muffler drops. It can be seen that the temperatures of the mufflers, in both Figs. 5 and 6, approach a steady value while the input current is still being applied. It will be shown later that this final temperature is proportional to the Peltier coefficient, resistance, and thermal conductivity of the TEMs

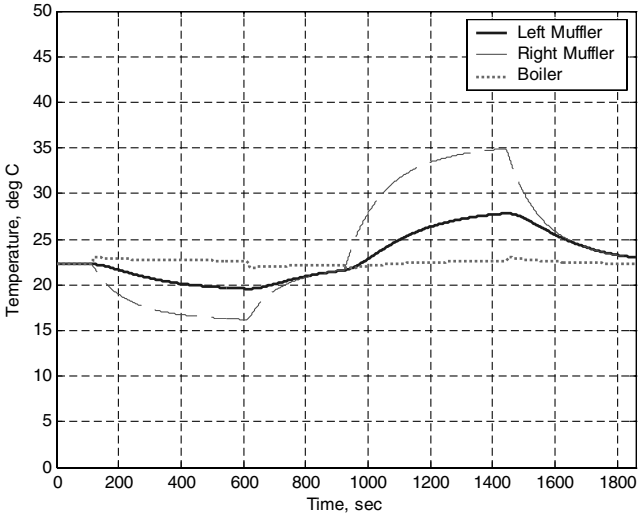

Fig. 6 Temperature response resulting from case 2 input current profile.

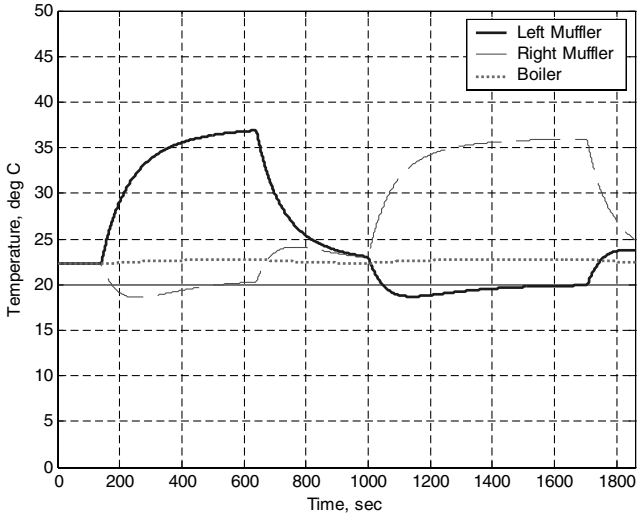

Fig. 7 Temperature response resulting from case 3 input current profile.

themselves. Again the temperature of the left muffler is also slightly affected by the input current in the right TEM bank.

C. Case 3—Shuttle TEM Bank Actuated

The final simple current profile evaluates the temperature responses due to activation of the shuttle TEM bank alone. The same current profile is input to the shuttle TEM bank with an initial positive current. The temperature response is shown in Fig. 7. In this case the muffler temperatures are both directly affected by the application of current, but the temperature of the boiler is only slightly affected.

D. Case 4—All TEM Banks Actuated Sequentially

A complex input current profile is the last case under investigation. This profile is shown below in Fig. 8, and the temperature response is shown in Fig. 9.

IV. Numerical Modeling

The experimental setup can be modeled as four thermal zones that transmit heat to one another in the fashion shown in Fig. 10. The mufflers and NiTinol tubes internal to each muffler are each taken to be one thermal zone, with the thermal-zone mass being the sum of the tubes, aluminum muffler, and half of each TEM row adjacent to the thermal zone. Similar lumped mass models have been proven in

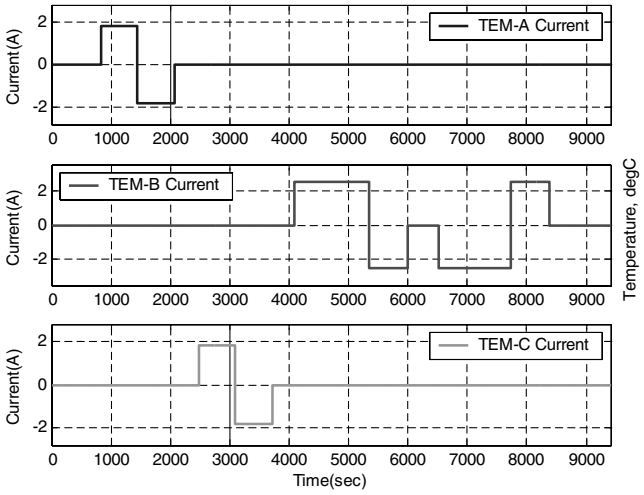

Fig. 8 Input current profile for case 4.

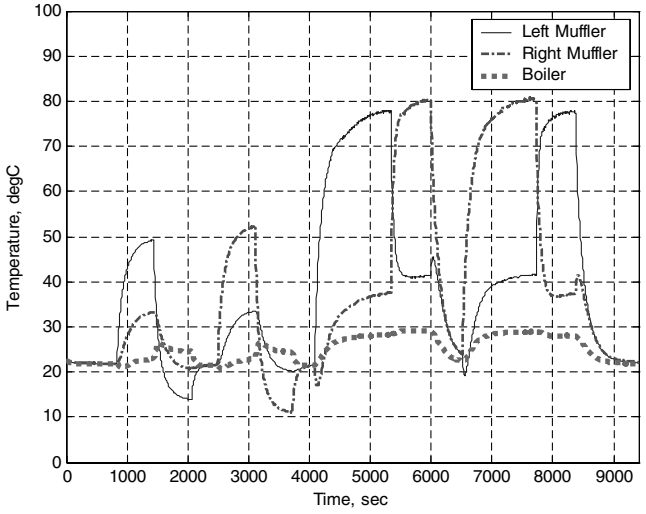

Fig. 9 Temperature response resulting from case 4 input current profile.

some cases to remove the necessity for more elaborate analysis techniques [3].

The specific heat of the thermal zone is taken to be the mass-averaged specific heat of its constituent parts. For the case of the NiTinol, however, there is a strong temperature dependence of the specific heat, as shown in Fig. 11. These data were acquired experimentally and show a significant specific heat capacity peak around 70°C. The final thermal-zone specific heat then becomes a function of temperature for the zones containing NiTinol (1 and 2). The outer thermal zones (3 and 4) represent the boiler. The mass of each of these zones is taken to be half of the boiler mass plus half of the mass of the adjacent TEM rows. Separating the boiler into two disconnected thermal zones takes into consideration the fact that conduction from the inboard portion to the outboard portion of the boiler is negligible and takes a long time in comparison to the heat transfer from the adjacent TEMs. A more accurate thermal model

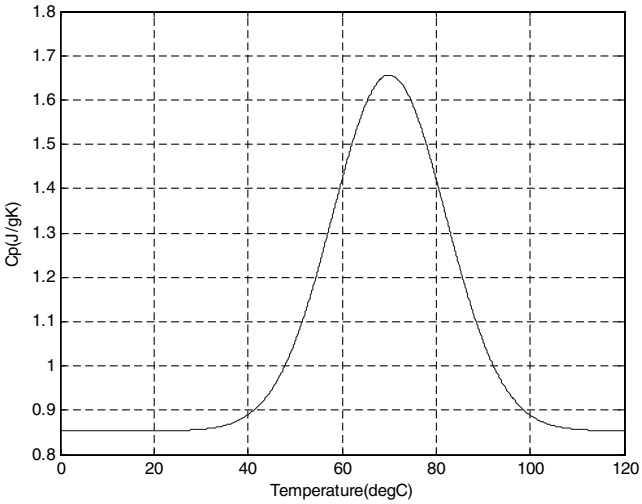

Fig. 11 Temperature dependence of NiTinol specific heat capacity.

will either consider these two thermal zones to be the same or have an additional thermal zone connecting the two and properly portioning the mass between the three zones. The specific heats of the boiler zones are also taken to be the mass-averaged specific heats of their constituent parts. In the case of the boiler zones there is no temperature dependency.

The heat balance at any given point in the model can be given by the following equation:

$$mc_p \frac{\partial T}{\partial t} = \sum q_i \tag{1}$$

The TEM model consists of two temperature zones, one for each side of the TEM. Each of the two zone equations contains three terms on the right, as shown below. The subscript 1 describes the thermal zone on the left of a TEM, and the subscript 2 refers to the thermal zone on the right:

$$m_1 Cp_1 \frac{\partial T_1}{\partial t} = \alpha I T_1 + \frac{1}{2} RI^2 - \kappa (T_1 - T_2) \tag{2}$$

$$m_2 Cp_2 \frac{\partial T_2}{\partial T} = -\alpha I T_2 + \frac{1}{2} RI^2 + \kappa (T_1 - T_2) \tag{3}$$

The temperature change experienced by the thermal zone is governed by three heat flows. The first term, involving α, is the pumped heat described by the Peltier effect. The second term represents the heat source term due to the resistance heating of the TEM and is proportional to the square of the input current. The final term is the heat flow due to conduction that occurs when there is a temperature difference across the TEM.

In a similar fashion, we have applied Eq. (1) to each of the four zones shown in Fig. 10 to develop the following four equations:

$$m_1 Cp_1 \frac{\partial T_1}{\partial t} = (N_b \alpha_b I_b + N_a \alpha_a I_a) T_1 + \frac{1}{2}(N_b R_b I_b^2 + N_a R_a I_a^2) + [N_a \kappa_a (T_3 - T_1) - N_b \kappa_b (T_1 - T_2)] \tag{4}$$

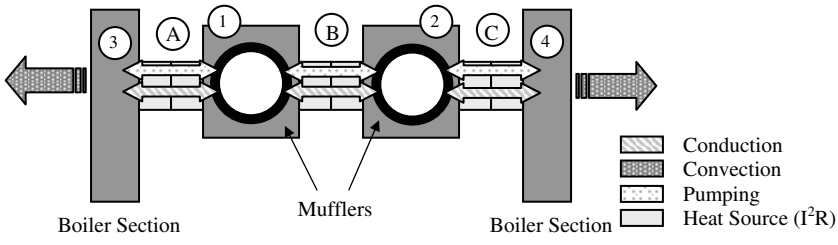

Fig. 10 Four-zone thermal model.

$$m_2 Cp_2 \frac{\partial T_2}{\partial t} = (N_c \alpha_c I_c - N_b \alpha_b I_b) T_2 + \frac{1}{2}(N_b R_b I_b^2 + N_c R_c I_c^2) + [N_b \kappa_b (T_1 - T_2) - N_c \kappa_c (T_2 - T_4)] \quad (5)$$

$$m_3 Cp_3 \frac{\partial T_3}{\partial t} = -N_a \alpha_a I_a T_3 + \frac{1}{2} N_a R_a I_a^2 - N_a \kappa_a (T_3 - T_1) - h_3 (T_3 - T_{\text{air}}) \quad (6)$$

$$m_4 Cp_4 \frac{\partial T_4}{\partial t} = -N_c \alpha_c I_c T_4 + \frac{1}{2} N_c R_c I_c^2 + N_c \kappa_c (T_2 - T_4) - h_4 (T_4 - T_{\text{air}}) \quad (7)$$

It must be noted here that the nomenclature is defined such that a positive current in the left bank of TEMs 1) will result in heat being pumped from zone 3 to zone 1, a positive current in the shuttle bank of TEMs; 2) will result in heat being pumped from zone 2 to zone 1, and a positive current in the right guard bank of TEMs; 3) will result in heat being pumped from zone 4 to zone 2. Additionally, convection will be investigated from zones 3 and 4, with a heat transfer coefficient h being applied to each of these zones proportional to the difference in the zone temperature and the ambient temperature. The temperature dependency of the NiTinol material is incorporated as a high-order polynomial fit to the trend shown in Fig. 11, with the model finding the appropriate value to use at each temperature by using this function.

Using a first-order forward finite difference to replace the time derivatives, knowing the initial system temperatures and the input current profiles, leads to a completely described system with four equations and four unknown temperatures (T_{1-4}) [4]. A grid independence study shows that a time step of $\Delta t = 0.5$ s is more than sufficient to simulate the system, as even cases simulated with larger time steps exhibited no grid dependency.

V. Sensitivity Analysis

The purpose of this examination is to see how the simulation responds to variations in each of the system parameters, including convective heat transfer coefficient, specific heat capacity, electrical resistance, and thermal conductivity, from a specific baseline value. As such, simulations are performed using the governing equations described above, varying one parameter at a time to quantify the sensitivity of the model to this variable. Because the model being used is greatly simplified over the physical system, variations in the TEM parameters from their actual values may be used to make up the deficiencies of the numerical model. Finding these optimized values for one case and quantifying their success on other cases will demonstrate the overall success of this methodology. TEMs used in the experimental setup were provided with manufacturer information pertaining to these numbers; however, experimental measurements showed a significant variation from these baselines, which were magnified with use. Baseline values for each of the pertinent TEM variables is shown in Table 1, while the baseline value of the specific heat capacity of the NiTinol material was taken to be temperature dependent as shown in Fig. 11.

Several cases were run on the most complex input current case, each varying a specific parameter from this baseline. The root-mean-square error between the simulation and the experimental results were computed in each case and plotted against the variation from the baseline values to determine which values of these parameters lead to the most precise representation of the experimental setup. For example, the rms error of the temperature difference between two thermal zones is found as

$$\varepsilon_{T,\text{rms}} = \sqrt{\frac{\sum_{i=0}^{n} [\Delta T_{\text{simulation}}(i) - \Delta T_{\text{measured}}(i)]^2}{n}} \quad (8)$$

where ΔT is the temperature difference between two adjacent thermal zones. Likewise, the maximum temperature difference between two thermal zones is computed by the following equation:

$$\Delta T_{\max} = \max_{i=0}^{n} [\Delta T_{\text{simulation}}(i) - T_{\text{measured}}(i)] \quad (9)$$

The first parametric study allowed the specific heat capacity of the NiTinol material to vary from the baseline value first measured experimentally before the system was built. For this study the TEM resistance was held constant at a value 75% larger than its baseline, the Peltier coefficient was 25% lower for all TEM banks, the thermal conductivity of the two guard banks was reduced 25%, and the convection from the boiler zones was maintained at 3.50 W/K. It was found that increasing the specific heat capacity by 25% at all temperatures led to the smallest rms error between the experimental results and the simulation results, approximately 3.88°C, as shown in Fig. 12. On the other hand the minimization of the maximum temperature difference between the experimental and simulation results occurred with only a 10% increase in the specific heat capacity of the NiTinol material. This turns out to be a difference of 10.66°C, but the large temperature difference occurs for only a small duration of time. Unoptimized simulations showed that the time constant for temperature change were smaller than those indicated by the experimental results. This suggested that the specific heat capacity was too small, and it should be increased to provide a better match to the data.

The next variable under investigation was the thermal conductivity of the TEMs. While the optimized NiTinol specific heat capacity of 25% over the baseline was used, the resistance and Peltier coefficients were kept at the values described in the previous section. A boiler heat transfer coefficient of 4.50 W/K was used, but further investigation of this variable is reported later. The conductivities of the left guard and right guard banks of TEMs were varied symmetrically, and in terms of rms error and maximum temperature differences the optimum conductivity to match the experimental results was 25% lower than those measured experimentally. Figure 13 shows that the minimized rms is approximately 3.86°C, and that the smallest temperature difference is 10.65°C. The reduced thermal conductivity in the left and right guard banks also makes sense due to the fact that when plotting the unoptimized simulation results, the temperature differences between the left muffler and boiler and the right muffler and boiler was too

Table 1 Baseline thermoelectric module coefficients

	Left guard TEMs	Shuttle TEMs	Right guard TEMs
Quantity	3	4	3
Total conductivity, W/K	0.468	0.275	0.529
Resistance, W	0.55	0.55	0.55
Peltier coefficient, V/K	0.00805	0.00805	0.00805
Total mass, g	6.03	8.04	6.03
Specific heat capacity, J/kg · K	592.04	592.04	592.04

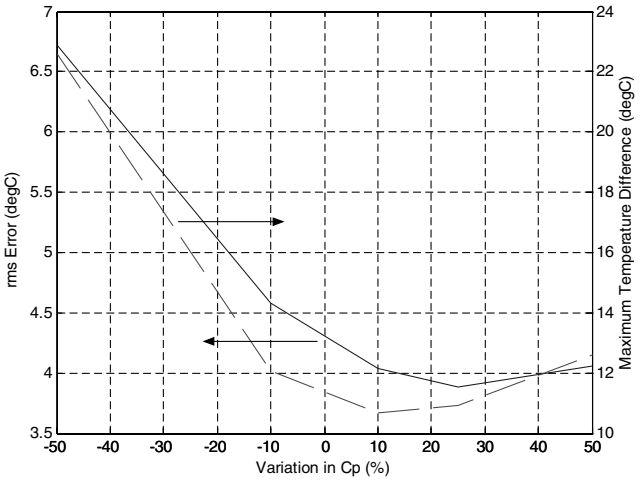

Fig. 12 Variation in rms error and maximum ΔT with Cp.

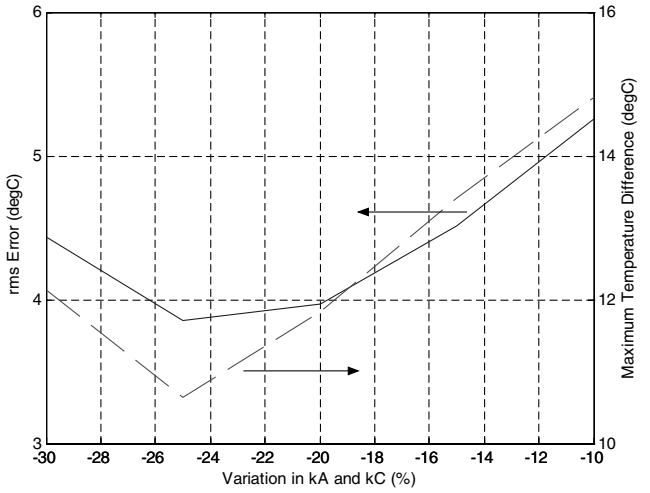

Fig. 13 Variation in rms error and maximum ΔT with κ_A and κ_C.

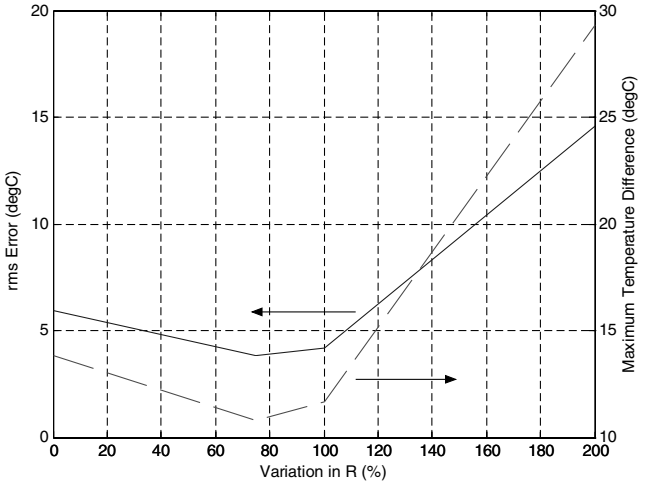

Fig. 14 Variation in rms error and maximum ΔT with TEM resistance.

large. Therefore reducing the constant of proportionality of these differences led to the optimized simulation parameters.

Using the same values described above with the optimized thermal conductivities, the electrical resistance was the next parameter varied, in large part due to the wide discrepancy in resistance measurements taken on the TEMs over time. As can be seen in Fig. 14, the rms is minimized when the resistance is taken to be 75% larger than its baseline value, leading to an rms error of 3.85°C. Likewise, the maximum temperature difference is minimized at this same increased resistance value, down to 10.79°C. It can be seen that increasing the resistance beyond this leads to much larger temperature differences.

The final variable that was investigated was the convective heat transfer coefficient for the boiler sections. This value was not permitted to change asymmetrically between the two sides and is an important parameter to study largely because a baseline for this variable is not known, only an estimated range. Figure 15 shows the minimization of the rms error, which occurs for a heat transfer coefficient of 4.00 W/K with a value of 3.84°C. It can be seen that there is little variation in the rms error when the heat transfer coefficient is varied between 3.50 and 4.50 W/K. This is mainly due to the clustering of simulation runs performed around the optimum heat transfer coefficient. The maximum temperature difference occurs for a heat transfer coefficient of 4.25 W/K, with a value of 10.78°C. When the heat transfer coefficient is dropped below this optimal value, less heat is permitted to escape the system and the temperature difference increases. Once these optima were found, it was necessary to make sure that each value remained optimized when coupled with the others. In large part this turned out to be true,

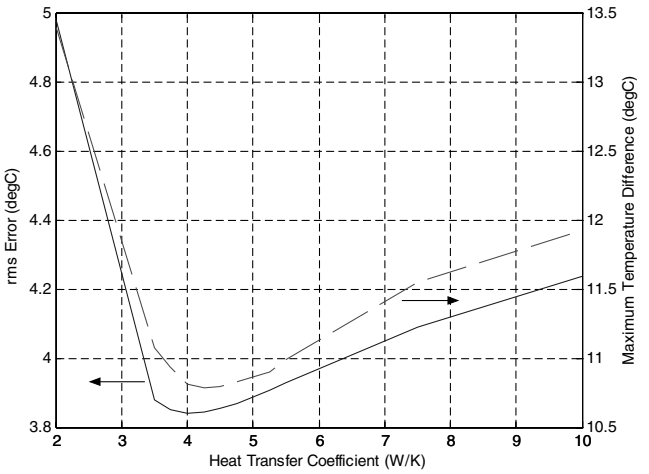

Fig. 15 Variation in rms error and maximum ΔT with heat transfer coefficient.

with the exception of the specific heat capacity. It had to be increased by 28% when combined with the other optimized parameters to become an optimized value.

The variations of each of these parameters from the baselines led to a better comparison between experimental and simulation results. This does not necessarily mean that the values of these parameters in the experimental setup have varied to this extent from their baseline values, but it may be that the variations required to best match the experiments in the simulation make up for modeling deficiencies.

VI. Simulation Results

After investigating the sensitivity of the model to each of the variables described in the previous section, the model was optimized to provide the best representation of the experimental results. Simulations were then run using optimized system variables and compared against all four cases to see how well the results could be compared. It was found in all cases that the qualitative data trends were well captured.

A. Case 1—Left Guard TEM Bank Actuated

Figure 16 shows the temperature of the left muffler as predicted by the four-zone model with optimized system variables together with the experimental results. It can be seen that the model predicts the behavior of this part of the system extremely well. For this thermal zone, the rms error between the model and the experimental results is only 1.40°C, with a maximum temperature difference of 2.74°C. The

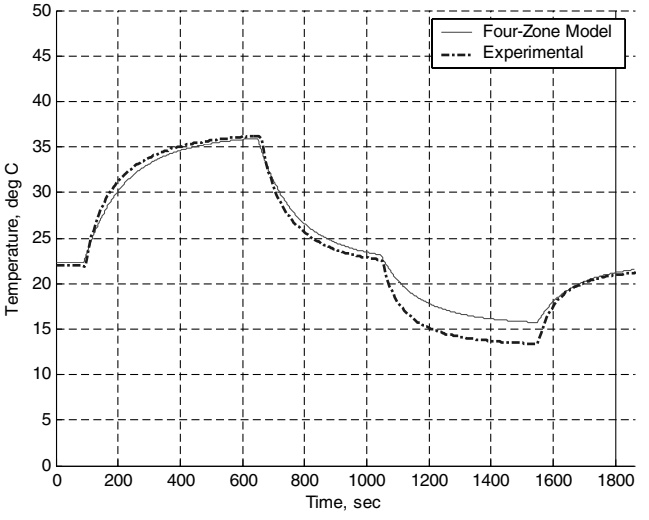

Fig. 16 Left muffler temperature response.

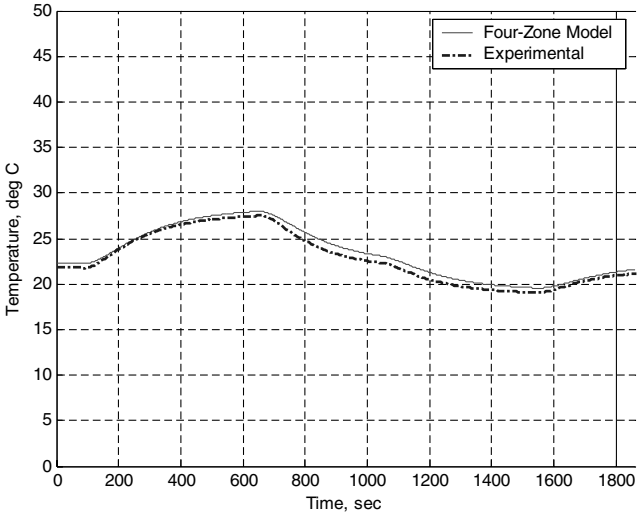

Fig. 17 Right muffler temperature response.

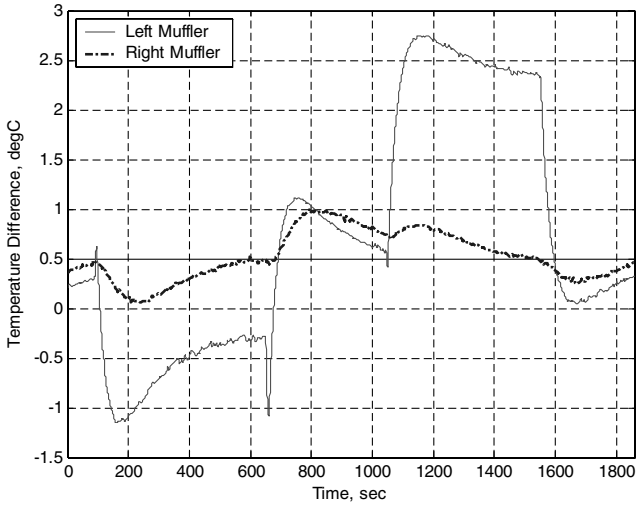

Fig. 18 Error in temperature prediction for case 1.

comparison between the prediction and experimental results for the right muffler is shown in Fig. 17. The prediction matches well the thermocouple data, with an rms error of 0.58°C and a maximum temperature error of 1.00°C. As described in the Experimental Results section, because the left bank of actuators was supplied with current, only a slight temperature shift is felt in the right muffler. The error for case 1 is shown in Fig. 18. It is clear from this figure that the errors are not random. They are most probably the result of inadequacies in the four-zone thermal model. The model does not account for convective losses from the tops of the mufflers, or asymmetric system variables such as electrical resistance, as well as numerous other heat sinks. Nevertheless, this degree of accuracy is found to be acceptable for such a simplified model.

B. Case 2—Right Guard TEM Bank Actuated

Similarly, Fig. 19 shows the left muffler temperature as predicted by the four-zone model using the same optimized system variables, plotted alongside the experimental results. A small temperature variation is experienced in the left muffler since the far bank of TEMs is being actuated. For this thermal zone, the rms error between the model and the experimental results is only 0.46°C, with a maximum temperature difference of 0.65°C. Figure 20 shows the comparison between the prediction and experimental results for the right muffler. Again the prediction matches the thermocouple data, with an rms error of 1.78°C and a maximum temperature error of 3.24°C at approximately 200 s, as indicated in Fig. 21.

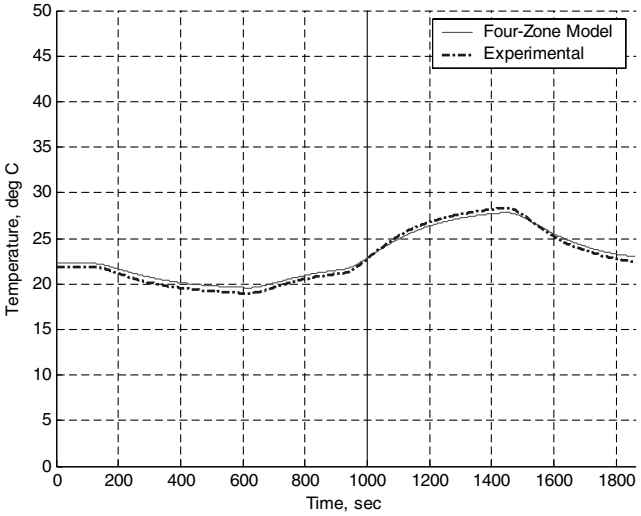

Fig. 19 Left muffler temperature response.

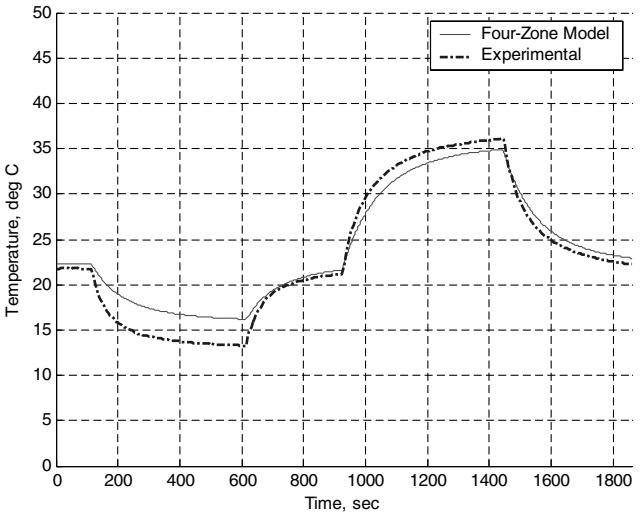

Fig. 20 Right muffler temperature response.

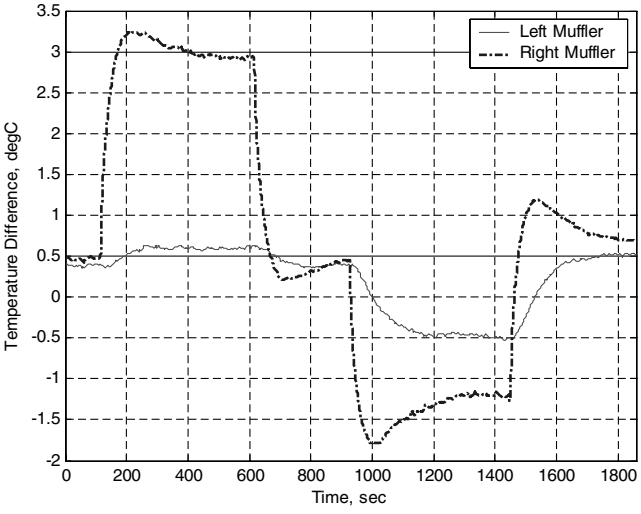

Fig. 21 Error in temperature prediction for case 2.

C. Case 3—Shuttle TEM Bank Actuated

Figure 22 shows the temperature of the left muffler for the case in which the shuttle bank of TEMs is powered. The model predictions for this thermal zone show an rms error between the model and the experimental results of only 1.15°C, with a maximum temperature

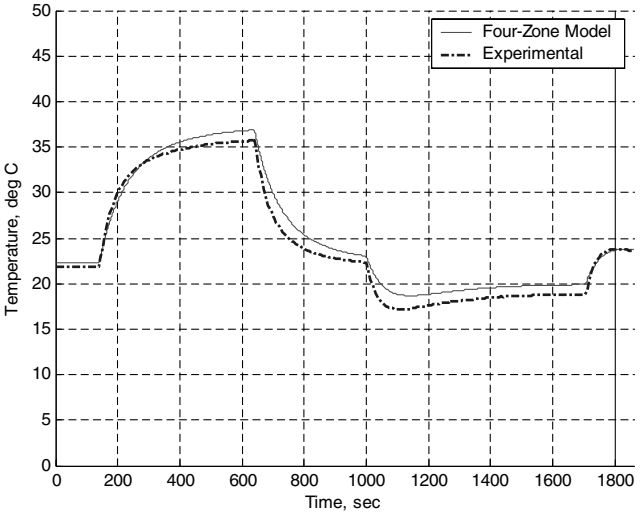

Fig. 22 Left muffler temperature response.

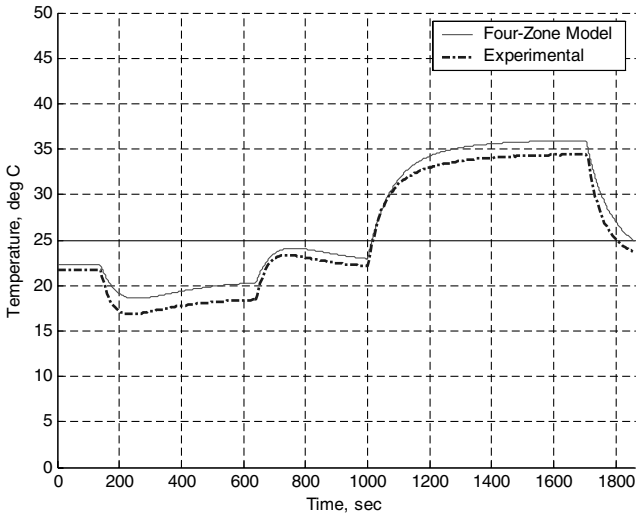

Fig. 23 Right muffler temperature response.

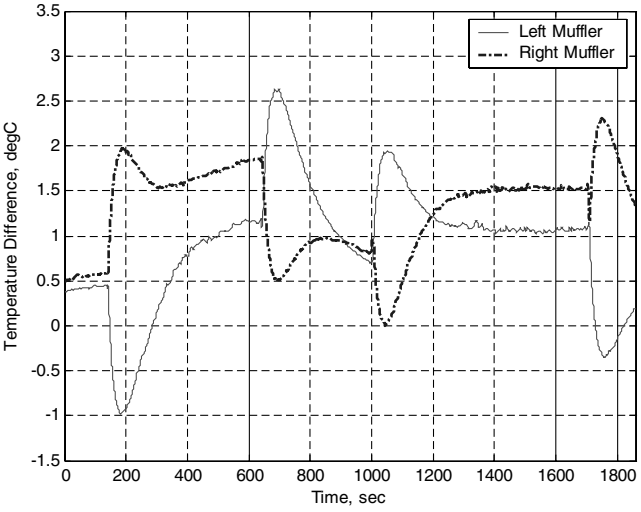

Fig. 24 Error in temperature prediction for case 3.

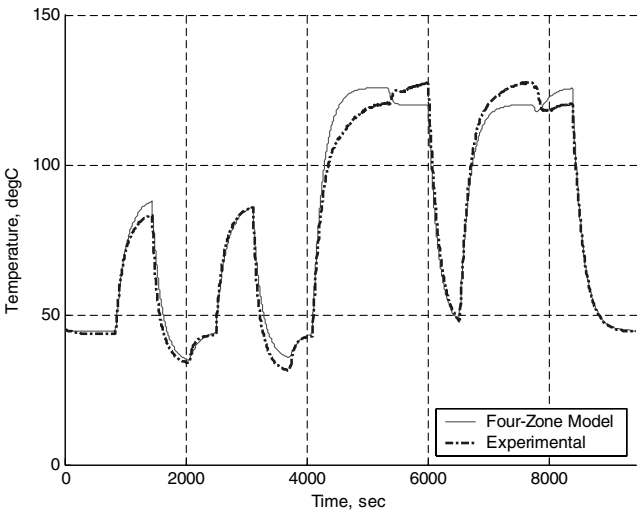

Fig. 25 Interior temperature summation, $T1 + T2$.

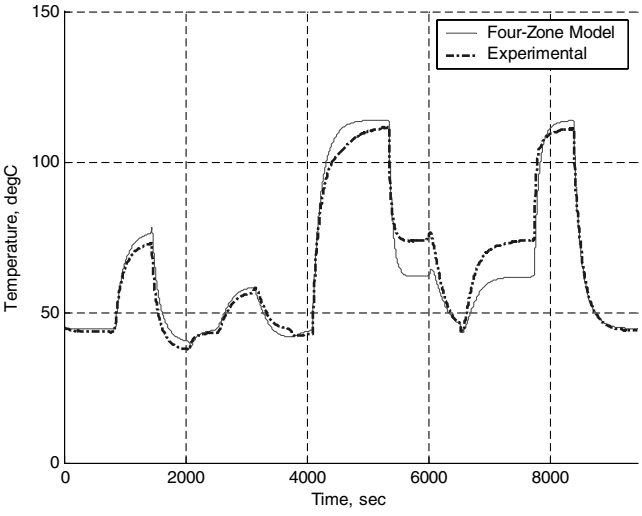

Fig. 26 Left side temperature summation, $T1 + T3$.

difference of 2.63°C. The comparison between the prediction and experimental results of the right muffler are shown in Fig. 23. Again the prediction matches the thermocouple data with an rms error of 1.38°C and a maximum temperature error of 2.30°C. The error for case 3 is shown in Fig. 24.

D. Case 4—All TEM Banks Actuated Sequentially

The following plots will compare the experimental results to the simulation results for sums and differences of temperatures of adjacent thermal zones. By rearranging Eqs. (2) and (3) it can be shown that the influence of the thermal conductivity is eliminated in the temperature sum, and the influence of resistance heating is eliminated in the case of the temperature difference. Figure 25 shows the largest discrepancy during the times between 4200 and 5400 s, and again between 6800 and 8400 s. The first of these periods is near steady state for positive current, and the second is during a period of current reversal in the shuttle bank. The major discrepancies are also observed in the left side temperature summation shown in Fig. 26. The right side temperature summation, Fig. 27, does not indicate the same level of divergence. The discrepancy therefore appears to be located on the left side only and is associated with both positive and negative currents. This suggests that it involves summation parameters such as resistance and convective heat transfer coefficient. In this model the resistance is not allowed to vary between the TEM banks. It is likely, therefore, that the model results could be improved by adjusting the resistance and heat transfer coefficient of the left side slightly while holding the right side coefficients constant. The temperature-difference results are presented in Figs. 28–30. They show smaller discrepancies than the summation results, indicating that the Peltier and thermal conductivity terms are nearly correct. Still, systematic errors do appear that indicate that the left side is slightly different than the right, and these very terms could be the source of the discrepancies.

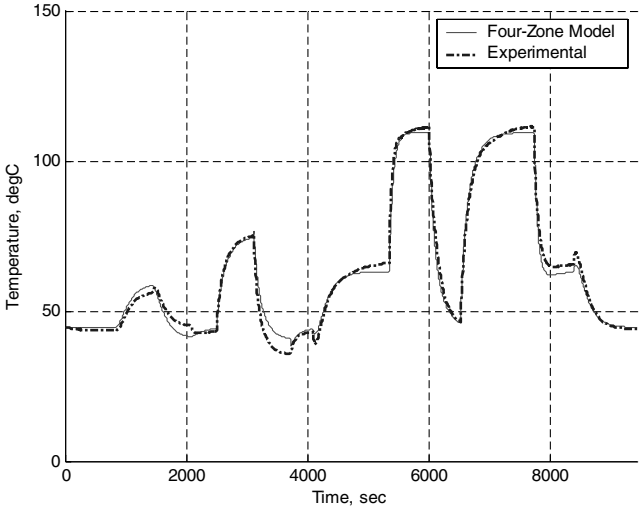

Fig. 27 Right side temperature summation, $T2 + T4$.

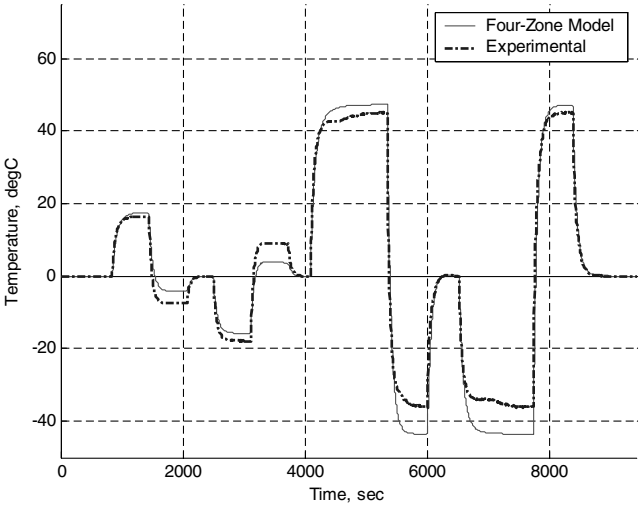

Fig. 28 Interior temperature difference, $T1 - T2$.

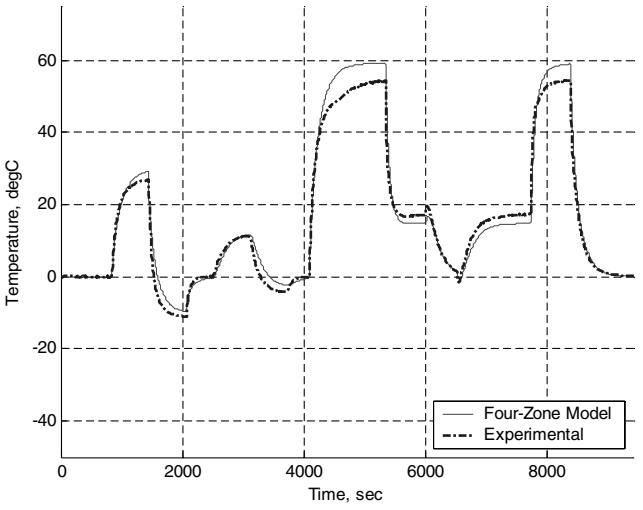

Fig. 29 Left side temperature difference, $T1 - T3$.

VII. Conclusions

Discrepancies between experimental and simulation results still exist, but most cases do not indicate a large level of divergence. Given that this model is an extreme simplification in that it does not allow asymmetric convective heat transfer coefficient, Peltier coefficient, or electrical resistance variation, the level of discrepancy between the two data sets is acceptable. The data trend is predicted extremely well considering the low computational cost associated with this model and above mentioned simplifications. It is likely that the model results could be improved by removing the requirement of system symmetry. Nevertheless, the model results reflect well the general behavior of this rather complex system.

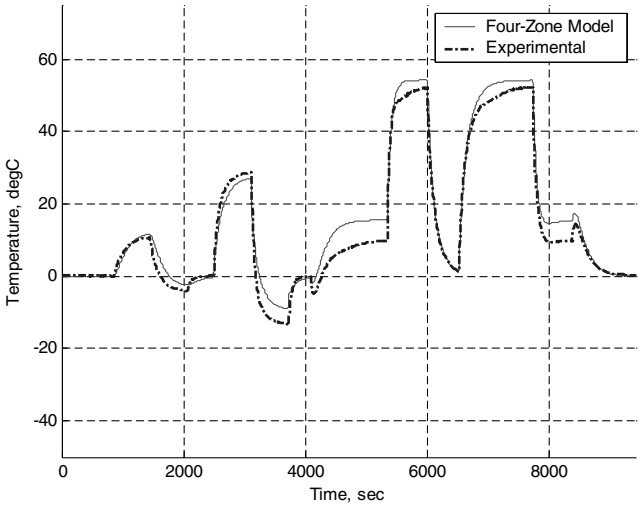

Fig. 30 Right side temperature difference, $T2 - T4$.

VIII. Future Work

One of the main focuses of future work is to remove the symmetry condition currently imposed in the thermal model. At this point, the only asymmetry included in the model is reflected in the different thermal conductivities of the guard TEM banks. This constraint may have major effects in terms of accurately predicting temperature histories. Additionally, a 14-zone thermal model has been developed and is currently under investigation. Many more heat loss terms are included in this model, as well as breaking up the individual zones in the four-zone model. For example, convection from the tops of the mufflers is included, as well as separating the NiTinol tubes from the mufflers into their own thermal zones. This actually simplifies matters in that the mufflers now have a constant specific heat capacity, while only the NiTinol tubes themselves have this temperature dependency. Although this more complex model adds many more variables into the system, it is expected that a better comparison of the experimental results will be available, and this model may be used to predict the system behavior on a full-scale flight system. Prior to that, more experimental data must be taken against which the predictions may be compared.

Acknowledgment

The authors would like to acknowledge the help of the technicians that assisted in performing the experimental work and collecting information on the thermoelectric modules that has helped to improve the simulation models.

References

[1] Ruggeri, R., Jacot, D., and Clingman, D., "Shape Memory Actuator Systems and The Use of Thermoelectric Modules," *Proceedings of the 9th SPIE Smart Structures and Materials Symposium*, SPIE, Bellingham, WA, 17–21 March 2002; also Paper 4698-386.

[2] Jacot, D., "Shape Memory Alloy Consortium," *Proceedings of the 6th SPIE Smart Structures and Materials Symposium*, SPIE, Bellingham, WA, 1–5 March 1999; also Paper 3674-018.

[3] Holman, J. P., *Heat Transfer*, 7th ed., McGraw–Hill, New York, 1999.

[4] Tannehill, J., Anderson, D., and Pletcher, R., *Computational Fluid Mechanics and Heat Transfer*, 2nd ed., Taylor and Francis Group, Philadelphia, PA, 1997.